Available online at www.sciencedirect.com

ScienceDirect

Procedia CIRP 111 (2022) 726–731

www.elsevier.com/locate/procedia

12th CIRP Conference on Photonic Technologies [LANE 2022], 4-8 September 2022, Fürth, Germany

Laser melt injection of spherical fused tungsten carbide in Cu-ETP with 515 nm wavelength laser

Anika Langebeck[a,*], Annika Bohlen[a], Thomas Seefeld[a], Xingxing Zhang[b], Joana Rebelo Kornmeier[b], Michael Hofmann[b], Shadi Alameddin[c], Renan Pereira Alessio[c], Felix Fritzen[c]

[a]*BIAS – Bremer Institut fuer angewandte Strahltechnik GmbH, Klagenfurter Strasse 5, 28359 Bremen, Germany*
[b]*Heinz Maier-Leibnitz Zentrum (MLZ), Technical University of Munich, Lichtenbergstrasse 1, 85748 Garching, Germany*
[c]*Stuttgart Center for Simulation Science, Institute of Applied Mechanics (CE), University of Stuttgart, Universitaetsstrasse 32, 70569 Stuttgart, Germany*

* Corresponding author. Tel.: +49-421-218-58035; fax: +49-421-218-58063. *E-mail address:* langebeck@bias.de

Abstract

Laser melt injection (LMI) is used to improve the wear resistance of highly loaded metal surfaces such as copper-based alloys for injection molds or casting tools. Therefore, a metal matrix composite (MMC) is formed by the injection of hard particles. When using copper as substrate material a laser with 515 nm wavelength is beneficial, due to its higher absorptivity. Nevertheless, the high thermal conductivity is a major challenge for a stable process and a MMC of high quality.
The present paper investigates the influence of substrate preheating for Cu-ETP and laser power on track geometry. Both parameters affect the thermal history and thus the residual stress of the MMC layer which is measured by neutron diffraction. The thermocycles are determined by two-color-pyrometry and tactile temperature measurements during both remelting and LMI with spherical fused tungsten carbide. These data were then used to validate a thermal simulation.

© 2022 The Authors. Published by Elsevier B.V.
This is an open access article under the CC BY-NC-ND license (https://creativecommons.org/licenses/by-nc-nd/4.0)
Peer-review under responsibility of the international review committee of the12th CIRP Conference on Photonic Technologies [LANE 2022]

Keywords: laser melt injection; metal matrix composite; tungsten carbide; copper; visible wavelength laser

1. Introduction

Laser melt injection (LMI) is a promising surface modification technology for highly loaded tools. With LMI metal matrix composites (MMC) with an advantageous combination of properties comprising high abrasive wear resistance due to the reinforcing hard particles and other properties depending on the matrix material, such as high thermal conductivity can be formed. These MMC surfaces are often used as protection layers against abrasive wear [1]. Therefore it can be beneficial for a variety of tools, such as casting tools and injection molds which are often made of copper alloys. However, laser processing of copper, especially pure copper like Cu-ETP, can be challenging due to its high thermal conductivity and a low absorptivity for conventional disk lasers with 1030 nm wavelength. To overcome this, preheating is beneficial [2]. Since a few years disk lasers with 515 nm wavelength and a maximum output power of several kilowatts are commercially available and used. With this wavelength Cu-ETP and other highly reflective materials can be processed more easily [3]. This enables more research in the field of laser processing of highly reflective materials, e.g. laser metal depostion [4] or LMI.

This work adresses a stable process window for remelting and especially LMI with Cu-ETP to study the influence of the process parameters on the MMC track geometry as well as the thermal history. The experimental data are then used to validate a thermal simulation of the remelting process. The thermal history and thus the LMI parameters will affect the thermal induced residual stress and distortions [5]. Therefore, the

2212-8271 © 2022 The Authors. Published by Elsevier B.V.
This is an open access article under the CC BY-NC-ND license (https://creativecommons.org/licenses/by-nc-nd/4.0)
Peer-review under responsibility of the international review committee of the12th CIRP Conference on Photonic Technologies [LANE 2022]
10.1016/j.procir.2022.08.071

This is a resupply of March 2023 as the template used in the publication of the original article contained errors. The content of the article has remained unaffected.

results shown in this paper are supplemented by residual stress measurements using neutron diffraction.

2. Experimental set-up and methods

2.1. Laser melt injection and remelting

For laser melt injection and remelting a Trumpf TruDisk 2021 laser with a wavelength of 515 nm and maximum output power of 2 kW was used. The beam was guided via a laser light cable with 600 µm core diameter to the processing head. The processing head has a collimation and focal length of 200 mm each. A discrete coaxial three-jet powder nozzle by Ixun with 16 mm working distance was used to carry the hard particles into the melt pool. To maintain a sufficient melt pool size for laser melt injection and remelting the laser beam was defocused to a spot diameter of 1.9 mm. Additionally, a heating plate by G. Maier Elektrotechnik was used to preheat the substrate before the laser process and was also used during the laser process.

As substrate material pure copper (Cu-ETP) with 50 mm length, 20 mm width and 12 mm height was used. Spherical fused tungsten carbide powder with a particle size of - 106 µm +45 µm was used. A Sensortherm Metis H322 two-color-pyrometer calibrated for temperatures between 700 °C and 2300 °C and a thermocouple type K were used simultaneously for the thermography. The pyrometer was moved together with the laser beam to monitor the temperature of the process zone. The thermocouple was embedded into the substrate via a small hole with 1.3 mm diameter, 3 mm underneath the surface (see Fig. 1 a)). It was used to measure the temperature near the process zone in the solid matrix material.

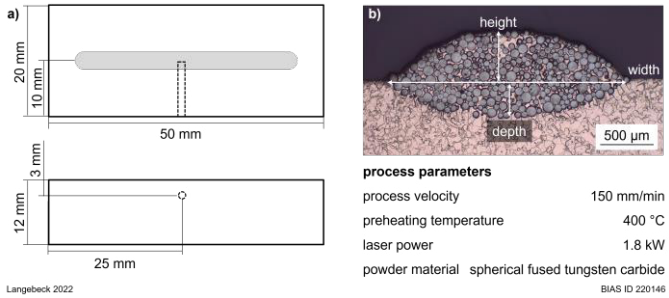

Fig. 1. a) Position of the thermocouple and b) MMC cross-section.

Laser power and preheating temperature were varied for both laser melt injection with spherical fused tungsten carbide and laser remelting without powder. Table 1 shows the examined parameter sets.

Multiple linear regression was used to describe the effect of laser power and preheating temperature on the MMC track geometry measured on the basis of cross-sections (see Fig. 1 b)). With the generated functions the effect of both varied parameters on the MMC track geometry (width, height and depth) can be calculated and compared.

Table 1. Parameter sets for laser melt injection and laser remelting.

Process parameter	Value(s)
Laser spot diameter	1.9 mm
Laser power	1.6 kW; 1.8 kW; 2.0 kW
Preheating temperature	300 °C; 400 °C
Process velocity	100 mm/min, 150 mm/min
Powder mass flow	5.5 g/min or none
Carrier gas (Ar)	3.5 l/min
Shielding gas (Ar)	15 l/min
Track length	40 mm
Surface condition	Glass bead blasted

2.2. Neutron diffraction

The residual strains and stresses in the Cu matrix of the MMC sample manufactured using laser power of 1.8 kW, preheating temperature of 400 °C, and process velocity of 150 mm/min were measured using neutron diffraction, which was conducted at the beamline HB-2B High Intensity Diffractometer for Residual stress Analysis (HIDRA) of the High Flux Isotope Reactor (HFIR) at Oak Ridge National Laboratory (ORNL) [6]. The Si (422) monochromator was selected, yielding a wavelength of 1.54 Å for neutron diffraction. The gauge volume of 15×0.5×0.5 mm^3 was used for the transversal and normal directions, and that of 2×1×1 mm^3 was used for the longitudinal direction. 17 points along the ON direction of the laser-processed brick sample were measured (Fig. 2 a)).

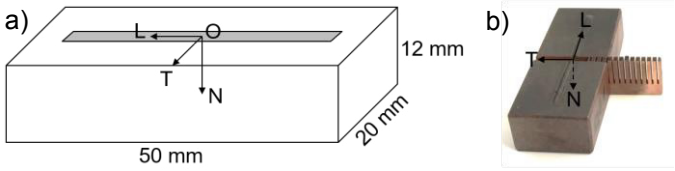

Fig. 2. a) The coordinate system O-L-T-N used for neutron diffraction. The origin point O locates at the top center of the processed track. 17 points along the ON direction were measured using neutron diffraction. b) A comb was cut using wire-electrode cutting from a twin sample for strain-free reference value measurement.

The strain-free reference values of the Cu matrix were measured using a comb sample (Fig. 2 b)). Each tooth of the comb is 2 mm in thickness and 1.8 mm in width.

The residual strains ε_i are calculated using

$$\varepsilon_i = \frac{\sin\theta_0}{\sin\theta_i} - 1 \quad (1)$$

where the subscript i denotes the longitudinal (L), transversal (T), and normal (N) direction, 2θ is the peak position, θ_0 the strain-free peak position of the comb sample, and θ_i is the peak position of the brick sample.

The tri-axial residual strains are then mapped to the tri-axial residual stresses using Hooke's law. The Cu (311) peak was selected for residual strain and stress analysis. The corresponding diffraction elastic modulus and Poisson's ratio of Cu (311) are 122.05 GPa and 0.352, respectively [7].

This is a resupply of March 2023 as the template used in the publication of the original article contained errors. The content of the article has remained unaffected.

2.3. Thermal Finite Element modeling

The modeling of the laser melt injection process is a challenging undertaking. In a first step, a finite element model was created within the commercial software LS-DYNA. Within this model, the remelting of a pure copper substrate without powder injection is mimicked. A Goldak moving heat source was employed [8]. The preheating of the substrate was modeled as an initial condition for the temperature. Boundary conditions were chosen based on variable convection coefficients on all surfaces. Although potentially a source of error, heat radiation was not considered in the first step in order to limit the number of unknown parameters to be calibrated. The calibration was pursued by fitting the simulations towards experimental measurements.

3. Results

3.1. Laser remelting

Fig. 3 shows exemplarily the temperature profile during remelting with 1.6 kW measured by a thermocouple (red line). In the temperature profile three different points t_0, t_1 and t_2 (red bars in Fig. 3) can be determined: the process start (Fig. 3, t_0) where the temperature increases above the preheating temperature of 400 °C, a change of the slope (Fig. 3, t_1) and the end of the process (Fig. 3, t_2) where the temperature decreases. The slope changes when the laser beam passes the thermocouple. In the first half of the diagram between t_0 and t_1 the leading heat towards the thermocouple is shown. In the second half between t_1 and t_2 the trailing heat towards the thermocouple is measured. The temperature profile for the LMI specimens in Sec. 3.2 is basically the same.

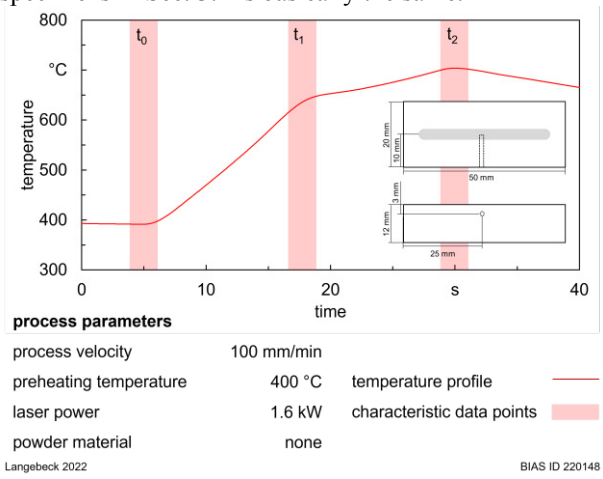

Fig. 3. Temperature profile during remelting measured by a thermocouple.

Fig. 4 shows in comparison to Fig. 3 the melt pool temperature measured by the two-color-pyrometer for the same specimen. During the first 5 s of the process an unstable temperature signal was detected. This corresponds to an unstable remelting which can be observed in the longitudinal section in Fig. 4 c). After this a more stable temperature signal was measured and a linearly increasing melt pool depth is observed (see Fig. 4, dashed violet line). The increasing melt pool depth correlates with a slightly increasing melt pool temperature. For higher laser power of 1.8 kW no unstable temperature signal was detected.

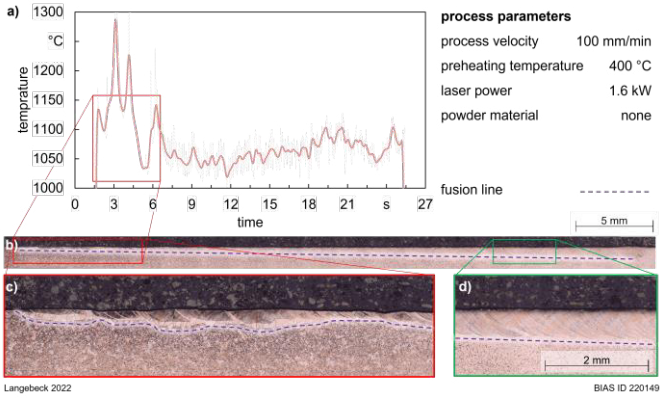

Fig. 4. a) Temperature profile during remelting measured by a two-color-pyrometer and b)-d) longitudinal sections.

The comparison of the modeled time history between t_0 and t_2 of the temperature at the position of the thermocouple with the experimental data for 1.6 kW and 1.8 kW is shown in Fig. 5. While material and process parameters are available with solid accuracy, a relevant yet unknown parameter was the laser absorption rate. In order to match the peak temperature measured at the thermocouple, an absorption rate of ~31% was identified for 1.8 kW laser power which also leads to matching time of the primary and secondary temperature peaks. The absorption rate will depend on, e.g., the boundary conditions or the finite element mesh, i.e., it may require further adjustments in the future.

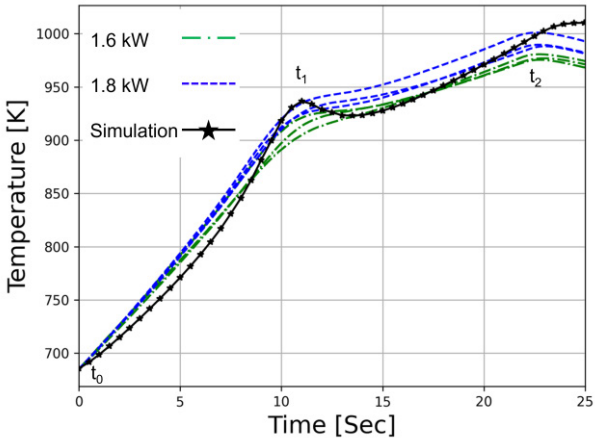

Fig. 5. Comparison of simulated and experimental temperature at the sub-surface thermocouple for laser power 1.8kW (blue) and 1.6 kW (green); three experiments are shown for each laser power to quantify experimental scatter.

This is a resupply of March 2023 as the template used in the publication of the original article contained errors. The content of the article has remained unaffected.

By looking at the modeled maximum temperature recorded at the top surface of the substrate, see Fig. 6, distinct heat accumulation towards the end of the process zone can be observed. This supports the experimental findings of a more profound remelting depth towards the end of the remelting process (see Fig. 4 b)-d)).

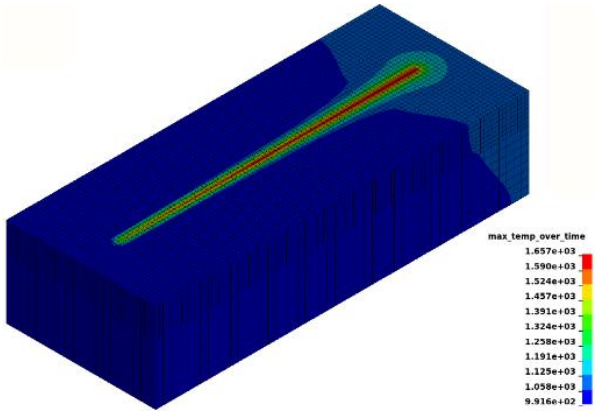

Fig. 6. Surface view of the maximum temperature during the process simulation; heat accumulation occurs at the end of the process zone (right top).

3.2. Laser melt injection

A stable process window for LMI in Cu-ETP with 515 nm wavelength laser was found (see Fig. 7). Except for the lowest laser power of 1.4 kW and lowest preheating temperature of 200 °C high quality MMC with a high particle content and a homogenous distribution with only a few pores were produced.

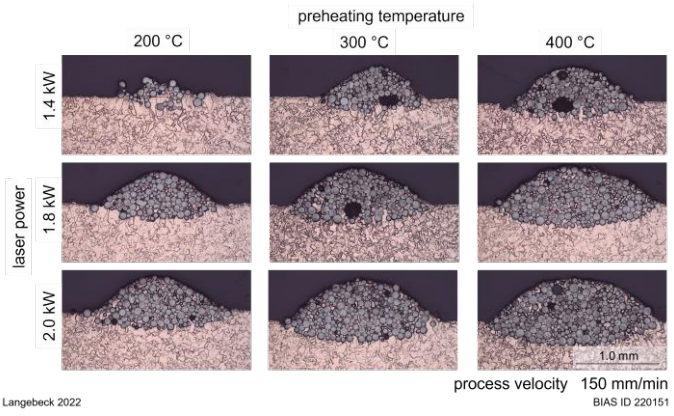

Fig. 7. Cross-sections of MMC tracks with different laser power and preheating temperature.

Fig. 8 shows the influence of the laser power and preheating temperature on the MMC track geometry. By increasing laser power and/or preheating temperature the MMC track geometry increases as well. A significant linear correlation between both parameters and the MMC geometry can be seen in the diagram and by using multiple linear regression.

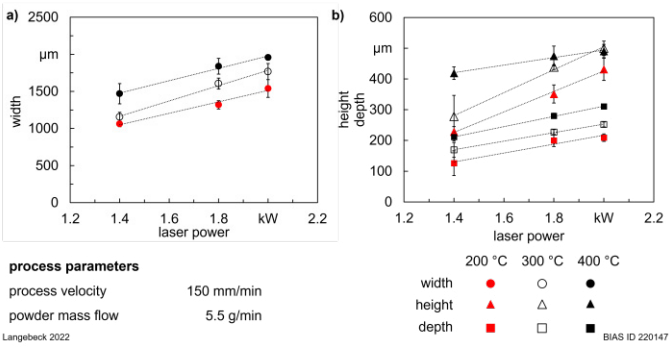

Fig. 8. MMC track a) width as well as b) height and depth depending on the process parameters laser power and preheating temperature.

The MMC track geometry can be estimated by three equations ((2) to (4)). X_{width} is MMC width, X_{height} is MMC height and X_{depth} is MMC depth. The variables T and P represent the used preheating temperature T in °C and laser power P in kW.

$$X_{width} = -825 + 2.35 * T + 962 * P \quad (2)$$
$$X_{height} = -134 + 0.421 * T + 238 * P \quad (3)$$
$$X_{depth} = -206 + 0.497 * T + 164 * P \quad (4)$$

Based on the linear equations (2) to (4) both parameters show the strongest effect on the MMC depth. For example, by increasing the laser power from 1.4 kW to 1.8 kW (at 200 °C) the depth increases by about 54%. In contrast, width and height will only increase by 34% to 39%. The same applies to the preheating temperature. An increase from 300 °C to 400 °C (at 1.4 kW) results in a 29% increased depth and only a 13% to 19% increased width and height.

Fig. 9 shows the results of the thermography, Fig. 9 a) displays the maximum temperature measured by the thermocouple directly underneath the MMC track and Fig. 9 b) shows the average temperature of the melt pool in the process zone. In the solid Cu-matrix peak temperatures between 516 °C and 628 °C where measured, which depend on the process parameters laser power and preheating temperature for both remelting without powder and laser melt injection with spherical fused tungsten carbide. Especially a higher preheating temperature (red marks vs. blue marks in Fig. 9 a)) leads to an increased maximum temperature in the solid Cu-ETP substrate during both laser processes. The effect of the laser power on the measured temperature depends on the preheating temperature. Whereas for the highest preheating temperature of 400 °C (red marks in Fig. 9 a)) a significant increase of the measured temperature from 590 °C to 628 °C for LMI and 579 °C to 602 °C for remelting was detected, only a slight but nonsignificant increase with increasing laser power at a lower preheating temperature of 300 °C (blue marks in Fig. 9 a)) was detected. In this case the measured peak temperature during LMI increases from 533 °C to 542 °C and during remelting from 516 °C to 523 °C. Apart from this the results show a significant effect of the powder. By supplying powder, the measured peak temperature during LMI increases

This is a resupply of March 2023 as the template used in the publication of the original article contained errors. The content of the article has remained unaffected.

about 2% to 4% in contrast to the remelting process without powder (see Fig. 9 a), filled circles vs. open circles).

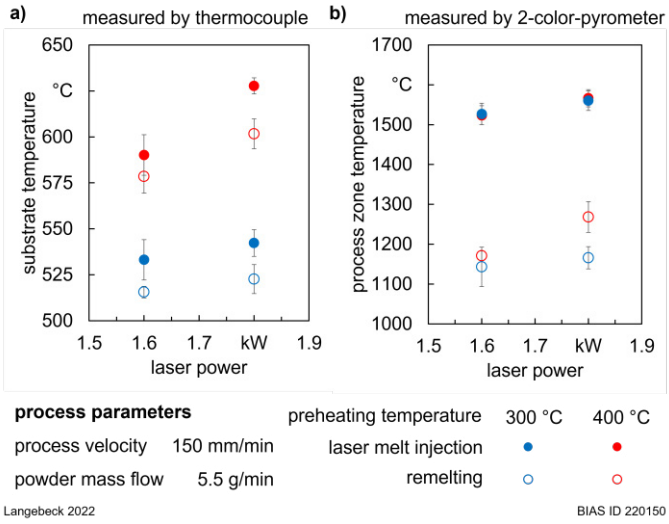

Fig. 9. a) Peak temperatures in the solid substrate measured by thermocouple and b) mean process zone temperature measured by two-color-pyrometer during LMI (filled circles) and remelting (open circles) depending on laser power and preheating temperature.

In contrast to the measurements by thermocouple of the solid substrate Fig. 9 b) shows the average melt pool temperature of 1143 °C to 1566 °C measured by the two-color-pyrometer depending on the process parameters. The data show a clear dependence of the average melt pool temperature on the powder supply. For the LMI process (filled circles) an average melt pool temperature between 1524 °C and 1566 °C was measured whereas for the remelting process (open circles) a significantly lower melt pool temperature between 1143 °C and 1269 °C was recorded. This trend was also monitored with the thermocouple (Fig. 9 a)). Unlike the measurements with the thermocouples, no impact of the preheating temperature on the average melt pool temperature during LMI could be detected with the two-color-pyrometer (filled circles in Fig. 9 b)). However, for remelting, the effect of preheating temperature and laser power was measured. Analogous to the results of the tactile temperature measurements, the average melt pool temperature increases with increasing laser power and preheating temperature.

3.3. Residual strains and residual stresses

The tri-axial residual strains in the Cu matrix of the MMC brick sample produced using laser power of 1.8 kW, preheating temperature of 400 °C, and process velocity of 150 mm/min are shown in Fig. 10 a). In general, the longitudinal residual strain (violet circles in Fig. 10 a)) is the highest and tensile, as expected, except at the depth of 7 mm. The residual strain state at the depth of 7 mm may be affected by its initial residual strains before the laser processing. Near the surface (depth of 0 mm), the longitudinal residual strains are about 200 to 320 micro-strains. The transversal residual strain is compressive, with the values varying from about -500 to -200 micro-strains. The normal residual strains at different locations are near zero. Correspondingly, the calculated residual stresses are shown in Fig. 10 b). The longitudinal residual stress at the depth of 0.7 mm is the highest, about 40 MPa. The transversal residual stress is compressive along with the depth, while the normal residual stress is near zero.

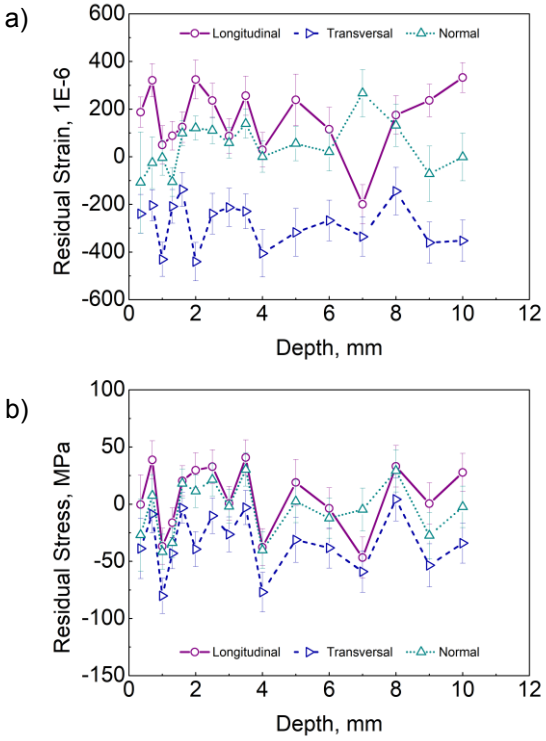

Fig. 10. a) Tri-axial residual strains and b) residual stresses along the depth direction.

4. Discussion

Both the laser power and the preheating temperature significantly influence the MMC geometry in Cu-ETP with spherical fused tungsten carbide. This was to be expected since both parameters directly affect the temperature profile of the specimens and thus also the melt pool geometry. The strongest effect was measured for the MMC depth. This is because towards the heating plate, in z-direction (= depth) the thermal conduction is slowed by a low temperature gradient between the melt pool and the bottom of the Cu-ETP substrate on the 400 °C or 300 °C hot heating plate. If the preheating temperature and/or the laser power are increased, the size of the melt pool increases. The effect of both process parameters on the temperature profile was investigated using tactile and thermographic measurement methods. In addition, the effect of the powder supply on the temperature profile was determined. Both measurement methods showed that for the material system investigated, the addition of the spherical fused tungsten carbide increased the process temperature. A reason for this is the absorption of the laser energy by the powder material [9]. Before the hard particles enter the melt pool they are heated by the laser and more energy is brought into the process zone. For the investigated Cu-ETP and spherical fused tungsten carbide material system, the additional energy input by the laser preheated powder is higher than the energy loss of the melt pool due to attenuation by the powder jet. The effect

This is a resupply of March 2023 as the template used in the publication of the original article contained errors. The content of the article has remained unaffected.

size depends on the material system and its absorptivity for the used laser wavelength.

The neutron diffraction experiment reveals that the magnitudes of residual stresses are small. This should be associated with two facts. On the one hand, a preheating temperature of 300 °C or 400 °C reduces the thermal gradient during the laser processing. On the other hand, the yield strength of Cu-ETP is relatively low at room temperature, about 75 MPa, and even lower at higher temperatures [10].

The predictive capabilities of the simulations were confirmed by the experimental data at hand. Interestingly, the available full-field temperature data on both the surface and within the bulk material as a function of time gives access to information that is hard to capture within experiments. For instance, the increased melt pool size towards the end of the process zone is predicted by the thermal simulations and an estimate of the depth of the melt pool can be gained from postprocessing the simulations.

5. Conclusion

For the first time it was shown that Cu-ETP based MMC of high quality can be manufactured using laser melt injection with a 515 nm wavelength laser. The higher absorption of approx. 30% for this wavelength enables a stable process window and MMC with only a few imperfections as well as a homogenous and high hard particle content were produced. With increasing laser power and/or preheating temperature the MMC track increases in width, depth, and height, whereas the effect on the MMC depth was the strongest. The thermal history caused by these parameters can be successfully mapped by two-color-pyrometry and tactile measurements which validated the thermal simulation of the remelting process. Based on the current model, accurate simulations that account for powder injection can be realized in the future. For the first time neutron diffraction on Cu-ETP based MMC where conducted. The measurements show that with preheating the substrate, the residual stress in the MMC track can be reduced by large.

Acknowledgements

The IGF-Project with the IGF-No.: 21079 N / DVS-No.: 06.3341 of the “Forschungsvereinigung Schweißen und verwandte Verfahren e. V.” of the German Welding Society (DVS), Aachener Str. 172, 40223 Düsseldorf was funded by the Federal Ministry for Economic Affairs and Climate Action (BMWK) via the German Federation of Industrial Research Associations (AiF) in accordance with the policy to support the Industrial Collective Research (IGF) on the basis of a decision by the German Bundestag. Furthermore, the authors gratefully acknowledge the collaboration with the members of the project affiliated committee regarding the support of knowledge, material and equipment over the course of the research. The neutron diffraction experiment of this research used resources at the High Flux Isotope Reactor, a DOE Office of Science User Facility operated by the Oak Ridge National Laboratory. Felix Fritzen is funded by the Deutsche Forschungsgemeinschaft (DFG, German Research Foundation) under Germany‘s Excellence Strategy – EXC-2075 – project number 390740016 and within the Heisenberg program – FR2702/8 – project number 406068690. Shadi Alameddin and Felix Fritzen acknowledge the support by the Stuttgart Center for Simulation Science (SimTech).

The “BIAS ID” nos. are part of the figures and allow the retraceability of the results with respect to mandatory documentation required by the funding organization.

Supported by:

Federal Ministry for Economic Affairs and Climate Action

on the basis of a decision by the German Bundestag

AiF IGF DVS FORSCHUNG

References

[1] Zou Y, Tan C, Qiu Z, Ma W, Kuang M, Zeng D. Additively manufactured SiC-reinforced stainless steel with excellent strength and wear resistance. Additive Manufacturing 2021;41(1):101971. https://doi.org/10.1016/j.addma.2021.101971.

[2] Auwal ST, Ramesh S, Yusof F, Manladan SM. A review on laser beam welding of copper alloys. Int J Adv Manuf Technol 2018;96(1-4):475–90. https://doi.org/10.1007/s00170-017-1566-5.

[3] Alter L, Heider A, Bergmann J-P. Investigations on copper welding using a frequency-doubled disk laser and high welding speeds. Procedia CIRP 2018;74:12–6. https://doi.org/10.1016/j.procir.2018.08.003.

[4] Polenz S, Kolbe C, Bittner F, López E, Brückner F, Leyens C. Integration of pure copper to optimize heat dissipation in injection mould inserts using laser metal deposition. Journal of Laser Applications 2021;33(1):12029. https://doi.org/10.2351/7.0000303.

[5] Plati A, Tan JC, Golosnoy IO, Persoons R, van Acker K, Clyne TW. Residual Stress Generation during Laser Cladding of Steel with a Particulate Metal Matrix Composite. Adv. Eng. Mater. 2006;8(7):619–24. https://doi.org/10.1002/adem.200600063.

[6] Cornwell P, Bunn J, Fancher CM, Payzant EA, Hubbard CR. Current capabilities of the residual stress diffractometer at the high flux isotope reactor. Rev Sci Instrum 2018;89(9):92804. https://doi.org/10.1063/1.5037593.

[7] Zhang Y, Chen W, McDowell DL, Wang YM, Zhu T. Lattice strains and diffraction elastic constants of cubic polycrystals. Journal of the Mechanics and Physics of Solids 2020;138:103899. https://doi.org/10.1016/j.jmps.2020.103899.

[8] Goldak JA, Akhlaghi M. Computational Welding Mechanics. Springer Science & Business Media; 2005.

[9] Tan H, Fang Y, Zhong C, Yuan Z, Fan W, Li Z et al. Investigation of heating behavior of laser beam on powder stream in directed energy deposition. Surface and Coatings Technology 2020;397:126061. https://doi.org/10.1016/j.surfcoat.2020.126061.

[10] Jin L-Z, Sandström R. Numerical simulation of residual stresses for friction stir welds in copper canisters. Journal of Manufacturing Processes 2012;14(1):71–81. https://doi.org/10.1016/j.jmapro.2011.10.001.

This is a resupply of March 2023 as the template used in the publication of the original article contained errors. The content of the article has remained unaffected.